Modulation of multiply scattered coherent light by ultrasonic pulses: An analytical model

Sava Sakadžić and Lihong V. Wang
Optical Imaging Laboratory, Department of Biomedical Engineering, 3120 TAMU, Texas A&M University, College Station, Texas 77843-3120, USA
(Received 24 February 2005; published 30 September 2005)

We present an analytical solution for the acousto-optical modulation of multiply scattered light in a medium irradiated with a train of ultrasound pulses. Previous theory is extended to cases where the ultrasound-induced optical phase increments between the different scattering events are strongly correlated, and it is shown that the approximate similarity relation still holds. The relation between the ultrasound induced motions of the background fluid and the optical scatterers is generalized, and it is shown that correlation exists between the optical phase increments that are due to the scatterer movement and the optical phase increments that are due to the modulation of the optical index of refraction. Finally, it is shown that compared with the spectrum of ultrasound pulses, the power spectral density of acousto-optically modulated light is strongly attenuated at the higher ultrasound frequencies.

DOI: 10.1103/PhysRevE.72.036620 PACS number(s): 42.25.Dd, 42.90.+m

I. INTRODUCTION

The optical properties of soft biological tissues in the visible and near-infrared regions are related to the molecular structure of the tissues. Radiation at these wavelengths is nonionizing, and it has significant potential for the functional imaging and detection of tissue abnormalities. Much effort has been made to develop new soft tissue imaging modalities based on visible and near-infrared radiation.

Ultrasound-modulated optical tomography is a hybrid technique, proposed to provide better resolution for the optical imaging of soft biological tissues by combining ultrasonic resolution and optical contrast. In this technique [1,2], optical radiation, which has high temporal coherence, and ultrasound are applied simultaneously to soft biological tissue. The intensity of the ultrasound-modulated optical radiation is measured to provide information about the optical properties of the tissue region that is spatially localized by the interaction between the ultrasonic and electromagnetic waves.

In spite of a variety of different experimental configurations that have been invented to efficiently measure the ultrasonically modulated component of the optical intensity emerging from the biological tissue [2–15], the exact nature of the acousto-optical effect in a highly optically scattering medium is still not totally understood due to the complicated light-ultrasound interaction that occurs in the presence of optical scatterers. Approximate theories in the optical diffusion regime under a weak scattering approximation have been developed [3,4,16–18] that include one or both of the main mechanisms of modulation. Mechanism 1 is the optical phase variations that are due to the ultrasonically induced movement of the optical scatterers [3,4], and mechanism 2 is the optical phase variations that are due to ultrasonically induced changes in the optical index of refraction. Mechanism 2 was first modelled by Wang [16] combined with mechanism 1. Subsequently, the model was extended to account for anisotropic optical scattering, Brownian motion, and optical absorption [18]. Due to the limited number of physical configurations where the probability density function of the optical pathlength is analytically known, only slab transmission [16] and reflection [19] geometry have been analytically studied so far. However, the model can be easily incorporated into a Monte Carlo algorithm [17,18,20], offering the possibility of exploring a wide spectrum of geometries.

The existing theoretical model was developed for the interaction of a plane, monochromatic (CW) ultrasound wave with diffused light in an infinite scattering medium, neglecting the polarization effects. It is assumed that the ratio of the optical transport mean free path l_{tr} to the ultrasonic wavelength λ_a is large enough that the ultrasound induced optical phase increments associated with different scattering events are weakly correlated [4]. However, this assumption may not be valid in cases where broadband pulsed ultrasound is applied, which is a promising option for the development of soft tissue imaging technology based on the acousto-optical effect [11,13,14].

In this work, we extend present theory to cases where broadband ultrasound pulses interact with diffused light. In Sec. II A, we generalize the relation between the ultrasound induced optical scatterer movement and the fluid displacement in accordance with the analytical solution for a small rigid sphere oscillation in a viscous fluid. In Sec. II B, we develop an expression for the time averaged temporal autocorrelation function of the electrical field component associated with the optical paths of length s in turbid media, when an infinite train of ultrasonic pulses traverse the media. The approximate similarity relation is valid for a broad range of l_{tr}/λ_a values. We show that, in general, a correlation exists between the phase increments due to scatterer displacement and phase increments due to index of refraction changes even when the value of l_{tr}/λ_a is large. In Sec. III, we explore the influence of ultrasound frequencies on the behavior of acousto-optically modulated optical intensity. We also compare a simple heuristic Raman-Nath solution for the acousto-optical effect in a clear medium with our solution for the behavior of the modulated intensity. In Sec. IV, we present a complete solution for acousto-optical modulation for a few distinct profiles of ultrasound pulses in slab transmission and

reflection geometry. Finally, a summary of the results is presented.

II. TEMPORAL AUTOCORRELATION FUNCTION OF THE ELECTRICAL FIELD

A. Ultrasound induced movement of the optical scatterers

In general, the equations governing the ultrasound induced motion of a particle in a fluid are complex. In this work, we consider the oscillations of a small rigid spherical particle in a viscous flow, with no-slip conditions applied on the surface of the particle. It is assumed that the Reynolds number is much smaller than unity, and that the particle radius a_0 is smaller than the smallest scale in the flow. The Reynolds number is given by $a_0 W/\eta_k$, where η_k is the kinematic viscosity of the fluid, and W represents the amplitude of the relative sphere velocity in respect to the velocity of the surrounding fluid. These conditions are likely to be satisfied by optical scatterers in biological soft tissues, if we assume the ultrasound fields commonly generated in practice.

The equations derived for the general case of nonuniform flow [21,22] can be simplified significantly if we consider the plane ultrasonic wave and neglect the effect of gravity. In the latter case, the relation between the Fourier transform of fluid velocity $\tilde{u}(f)$ and the Fourier transform of particle velocity $\tilde{v}(f)$ is given by [23,24]

$$\tilde{v}(f) = \tilde{u}(f) Y(f_r, \gamma), \tag{1}$$

where

$$Y(f_r, \gamma) = \frac{1 - i f_r - (i-1)(3 f_r/2)^{1/2}}{1 - i(2\gamma+1) f_r/3 - (i-1)(3 f_r/2)^{1/2}}. \tag{2}$$

In Eq. (2), the relative ultrasonic frequency, $f_r = f/\nu_0$, is calculated in respect to $\nu_0 = 3\eta_k/(2\pi a_0^2)$; $i = \sqrt{-1}$ is the imaginary unit; and $\gamma = \hat{\rho}/\rho$ is the relative sphere density where $\hat{\rho}$ and ρ are densities of the sphere and the fluid, respectively. The Fourier transform of the function $c(t)$ is given by

$$\tilde{c}(f) = \int_{-\infty}^{+\infty} c(t) \exp(i 2\pi f t) dt. \tag{3}$$

As shown in Ref. [24], when the relative density of a particle such as an exogenous microbubble ultrasound contrast agent is low ($\gamma < 1$), the amplitude of the particle oscillation is greater than the amplitude of the fluid oscillation, and the phase of the particle oscillation precedes the phase of the fluid oscillation. However, in soft biological tissue, an endogenous optical scatterer has a density just slightly greater than the density of the surrounding medium. Also, the kinematic viscosity should be greater than, or equal to, the kinematic viscosity of water, which is approximately 10^{-6} m^2 s^{-1} at room temperature. In that case, the amplitude of the scatterer oscillation is slightly smaller than the amplitude of the medium oscillation, and the phase of the scatterer movement is slightly retarded in respect to the fluid movement. Therefore, the movement of the optical scatterer is expected to follow closely the movement of the surrounding fluid, although this model might be too simple to fully account for the complexities of real biological tissue.

B. Temporal autocorrelation function for the train of ultrasound pulses

In this model, we consider the independent multiple scattering of temporarily coherent diffused light in a scattering medium homogeneously filled with discrete optical scatterers in a general case of anisotropic optical scattering. We neglect the polarization effects and assume that the optical wavelength λ_0 is much smaller than the scattering mean free path l. We also assume that an ultrasonic plane wave is propagating unperturbed along the x axis without attenuation. The acoustical pressure in the medium is given by $P(\vec{r}, t) = P_0 f(x,t)$, where P_0 is the pressure amplitude, and the pressure propagation is represented by the function $f(x,t)$. Analogous to previous work [25,26] where the acousto-optical effect caused by pulsed ultrasound is analyzed in a clear medium, we assume that the pressure propagation function $f(x,t)$ represents an infinite train of ultrasound pulses

$$f(x,t) = \sum_{n=-\infty}^{+\infty} f_0(x - v_a t - n v_a T), \tag{4}$$

where v_a is the ultrasonic speed, and T is the time period between ultrasound pulses. The shape of the single ultrasonic pulse is given by function $f_0(x - v_a t)$.

The power spectral density (PSD) of the scattered light at the position of a point detector can be represented as

$$\mathcal{P}(\nu) = \int_{-\infty}^{+\infty} \Gamma(\tau) e^{i 2\pi\nu\tau} d\tau, \tag{5}$$

where $\Gamma(\tau)$ is the time averaged autocorrelation function of the electrical field [27].

We assume in this simple model that due to the weak scattering approximation ($l/\lambda_0 \gg 1$), the fields belonging to different random paths add incoherently to the average and that only photons traveling along the same path of length s contribute to the autocorrelation function [3,28–31]. Consequently, the time averaged autocorrelation function of the electrical field can be written as

$$\Gamma(\tau) = \int_0^{\infty} p(s) \Gamma_s(\tau) ds, \tag{6}$$

where $p(s)$ is the probability density function that the optical paths have length s, and $\Gamma_s(\tau)$ is the time averaged autocorrelation function of the electrical field associated with the paths of length s. We further assume the independence of the optical phase increments induced by the Brownian motion of the scatterers and those induced by ultrasound through mechanisms 1 and 2. Then, $\Gamma_s(\tau)$ can be represented as $\Gamma_{s,U}(\tau)\Gamma_{s,B}(\tau)$, where the indices B and U are associated with the Brownian motion and the ultrasonic effects, respectively. The influence of Brownian motion has been considered previously in the literature [18,19,28,29], and it can be expressed as $\Gamma_{s,B}(\tau) = \exp[-2s\tau/(l_{tr}\tau_0)]$, where l_{tr} is the optical

transport mean free path, and τ_0 is the single particle relaxation time.

To obtain the value of $\Gamma_{s,U}(\tau)$, we first consider phase φ_s of the electrical field component accumulated along the optical path of length s in optically diffusive media. The value of the electrical field component in the analytic signal representation is then proportional to $\exp[-i(\omega_0 t-\varphi_s)]$, where $\omega_0=2\pi f_0$, and f_0 is the optical frequency of the incident monochromatic light.

We assume that the perturbation of the dielectric permittivity of the medium due to the ultrasound is small and proportional to the ultrasound pressure. Consequently, perturbation of the optical index of refraction $n(x,t)$ due to ultrasound is also small and we have

$$n(x,t) \approx n_0\left[1+\tfrac{1}{2}Mf(x,t)\right]. \tag{7}$$

In Eq. (7), modulation coefficient M is equal to $2\eta P_0/\rho v_a^2$, and $\eta=\rho\partial n/\partial\rho$ is the elasto-optic coefficient (we assume for water $\eta\approx 0.32$). For soft biological tissues and for commonly applied ultrasonic pressures, the value of the modulation coefficient M is always much less than unity, which is in good agreement with the approximation we arrived at in Eq. (7).

For an optical path of length s, which begins at $\vec{r}_0$ and ends at $\vec{r}_{N+1}$ and has N scatterers at positions $\vec{r}_1,\ldots,\vec{r}_N$, the value of the accumulated optical phase calculated by integrating the index of refraction along the path is approximately equal to [16,18]

$$\varphi_{s,N} \approx k_0 n_0 \sum_{i=0}^{N} |\vec{r}_{i+1}-\vec{r}_i| + k_0 n_0 \sum_{i=1}^{N} (\chi_i-\chi_{i+1})\varepsilon_i(t) + k_0 n_0 \sum_{i=0}^{N} \frac{1}{2} M \int_{\vec{r}_i}^{\vec{r}_{i+1}} f(x,t)dr. \tag{8}$$

In Eq. (8), integrations in the last term are performed along the straight lines which connect consecutive scatterers; $k_0=2\pi/\lambda_0$ is the magnitude of the optical wave vector; $\chi_{i+1}=\cos(\theta_{i+1})$ where θ_{i+1} is the angle between ultrasound wavevector $\vec{k}_a$ and the vector $\vec{l}_{i+1}=\vec{r}_{i+1}-\vec{r}_i$ which connects two consecutive scatterers; and $\varepsilon_j(t)$ is the projection of the ultrasound induced displacement of the jth particle $\vec{\varepsilon}_j(t)$ at time t in the ultrasound propagation direction. Comparing Eq. (8) with the previous derivations [18], one more scatterer is included along the optical path for the convenience of the later averaging.

Several additional assumptions are included in Eq. (8). The ultrasound induced displacements of the scatterers are neglected in the limits of the integrals in the last term on the right-hand side of Eq. (8), which is a reasonable approximation when $k_0 n_0 M|\vec{\varepsilon}_j(t)| \ll 2$ and at the same time $|\vec{\varepsilon}_j(t)| \ll l$. In that way, the phase error due to the approximation is much smaller than one radian for each integral between two scatterers, and the total value of the error in each integration is much smaller than the integral itself, except in some cases where the value of the integral approaches zero due to increased phase cancellation when integrating occurs along the direction close to the ultrasound propagation direction. However, these cases contribute little to the total phase value. We also assume that the distance between consecutive scatterers can be approximated with $l_{i+1}+\chi_{i+1}[\varepsilon_{i+1}(t)-\varepsilon_i(t)]$, which is the case when $k_0 n_0 \varepsilon_i^2(t) \ll 2l$, and $|\varepsilon_i(t)| \ll l$. Finally, the accumulated phase $\varphi_{s,N}$ is calculated by integrating the optical phase increments along the straight lines which connect the scatterers along the optical path. Therefore, it is assumed that the distortion of the optical waves along the path between two consecutive scatterers due to ultrasound induced change in the optical index of refraction is negligible. Analogous to the Raman-Nath case of acousto-optical diffraction in clear media [32], we write this condition as $Q\nu_{\mathrm{RN}} \ll 1$, where $Q=lk_a^2/k_0$ and $\nu_{\mathrm{RN}}=k_0 l n_0 M/2$ are the Klein-Cook parameter and the Raman-Nath parameter, respectively. For the optical wavelengths in the visible and near-infrared regions in soft biological tissues and for common ultrasound pressures, the applied approximations limit the range of the ultrasound frequency values between $\approx$1 kHz and several tens of MHz. This can also be considered as a lower limit for the $k_a l$ product between 10^{-2} and 10^{-3}, and an upper limit for the $k_a l$ product around 100, depending on the precise values of the parameters.

We also assume in Eq. (8) that $\varepsilon_0(t)=\varepsilon_{N+1}(t)=0$, i.e., the displacements of the first and last scatterer (source and detector) are zero. It will be shown that this assumption is valid when the number of the scattering events along the path is very large, regardless of the value of the $k_a l$ product. However, when the $k_a l$ product is small, and N is as small as 10, ultrasound induced movement of the source and detector leads to a significant difference in effect due to mechanism 1.

Since the time invariant part associated with $|\vec{r}_{i+1}-\vec{r}_i|$ in Eq. (8) has no influence on the spectral properties of light, we consider only the other two terms, and write the ultrasound induced optical phase increment along the path as

$$\varphi_s(H,t) = k_0 n_0 \sum_{i=1}^{N} (\chi_i-\chi_{i+1})\varepsilon_i(t) + \frac{1}{2} k_0 n_0 M \sum_{i=0}^{N} \int_{\vec{r}_i}^{\vec{r}_{i+1}} f(\vec{r},t)dr, \tag{9}$$

In Eq. (9), term H represents the set of random variables $\{\vec{r}_0,\chi_1,l_1,\ldots,\chi_{N+1},l_{N+1}\}$ associated with the paths of length s with N scatterers. The probability density functions (PDF) of the first scatterer position and the cosines of the starting angle χ_1 are uniform. Also the PDF of the optical pathlength between two scattering events is given by $p(l_j)=l^{-1}\exp(-l_j/l)$, where l is the mean optical free path. Finally, the probability density of scattering a photon traveling in direction $\vec{e}_i=\vec{l}_i/l_i$ into direction $\vec{e}_{i+1}=\vec{l}_{i+1}/l_{i+1}$ is described with the phase function $g(\vec{e}_j\cdot\vec{e}_{j+1})$ which does not depend on the azimuth angle or the incident direction. The development of the phase function $g(\vec{e}_j\cdot\vec{e}_{j+1})$ over the Legendre polynomials $P_m(\vec{e}_j\cdot\vec{e}_{j+1})$ is given by

$$g(\vec{e}_j\cdot\vec{e}_{j+1}) = \sum_{m=0}^{\infty} \frac{2m+1}{2} g_m P_m(\vec{e}_j\cdot\vec{e}_{j+1}), \tag{10}$$

where $g_0=1$, and g_1 is the scattering anisotropy factor.

Now, we calculate the power spectral density of the optical intensity as a Fourier transform of the time averaged autocorrelation function [27]. It is interesting to note at this point that the random process associated with the sample functions $\varphi_s(H,t)$ is not wide sense stationary unless the diameter of the whole scattering volume is much larger than the ultrasound wavelength. In that case, averaging over $\vec{r}_0$ cancels the time dependence of the autocorrelation function.

We adopt the notation $\Delta\varphi_s=\varphi_s(H,t+\tau)-\varphi_s(H,t)$, such that the time averaged autocorrelation function $\Gamma_{s,U}(\tau)$ is expressed as

$$\Gamma_{s,U}(\tau)=\exp(-i\omega_0\tau)\langle\exp(i\Delta\varphi_s)\rangle_{t,H}. \tag{11}$$

In Eq. (11), $\langle\ \rangle_{t,H}$ represents averaging over time, and averaging over all of the random variables in H.

We proceed by representing the $\Delta\varphi_s$ with the help of Eq. (9), as

$$\Delta\varphi_s=\Delta\varphi_{s,n}+\Delta\varphi_{s,d}. \tag{12}$$

In Eq. (12), $\Delta\varphi_{s,n}$ is associated with index of refraction changes along the optical path

$$\Delta\varphi_{s,n}=\frac{1}{2}k_0n_0M\sum_{i=0}^{N}\int_{\vec{r}_i}^{\vec{r}_{i+1}}\Delta f(\vec{r},t,\tau)dr, \tag{13}$$

where $\Delta f(\vec{r},t,\tau)=f(\vec{r},t+\tau)-f(\vec{r},t)$. Similarly, term $\Delta\varphi_{s,d}$ on the right-hand side of Eq. (12) is associated with the ultrasound induced movement of the scatterers

$$\Delta\varphi_{s,d}=k_0n_0\sum_{j=1}^{N}(\chi_j-\chi_{j+1})\Delta\varepsilon_j(t,\tau), \tag{14}$$

where $\Delta\varepsilon_j(t,\tau)=\varepsilon_j(t+\tau)-\varepsilon_j(t)$.

Function $f(\vec{r},t)$ represents the acoustical pressure propagation [Eq. (4)]. Its representation using the Fourier spectral components is given by

$$f(x,t)=\frac{1}{v_aT}\sum_{n=-\infty}^{+\infty}\tilde{f}_0\left(\frac{n}{v_aT}\right)\exp[-in(k_ax-\omega_at)], \tag{15}$$

where $k_a=2\pi/(v_aT)$ and $\omega_a=2\pi/T$ are, respectively, the ultrasonic wave vector magnitude and the angular frequency associated with the period between ultrasonic pulses T. In Eq. (15), the Fourier transform $\tilde{f}_0(\nu)$ of the ultrasonic pulse shape function $f_0(x-v_at)$ is

$$\tilde{f}_0(\nu)=\int_{-\infty}^{+\infty}f_0(u)\exp[i2\pi\nu u]du. \tag{16}$$

To obtain the expression for the displacement of the scatterers, we assume that at each ultrasonic frequency f in a spectrum of the infinite train of ultrasonic pulses, the relation given by Eq. (1) is satisfied. For simplicity, we represent the variable $Y(f_r,\gamma)$ as a product $Y(f_r,\gamma)=S(f_r)\exp[i\phi(f_r)]$, where $S(f_r)$ is the amplitude and $\phi(f_r)$ is the phase of the scatterer velocity deviation from the fluid velocity. Then, the relation between the Fourier transforms of the scatterer velocity and the fluid velocity becomes

$$\tilde{v}(f)=\tilde{u}(f)S(f_r)\exp[i\phi(f_r)]. \tag{17}$$

In further derivations, we will denote with S_n and ϕ_n the values of $S(f_r)$ and $\phi(f_r)$ at ultrasound frequencies equal to $f_n=n/T$.

Using Eqs. (17) and (16), and assuming that the velocity of the fluid is given by $P(x,t)/(\rho v_a)$, we express the displacement of the jth scatterer as

$$\varepsilon_j(t)=-\frac{iP_0}{2\pi\rho v_a^2}\sum_{\substack{n=-\infty\\ n\neq0}}^{+\infty}\tilde{f}_0\left(\frac{n}{v_aT}\right)\frac{S_n\exp(-i\phi_n)}{n}\times\exp[-in(k_ax_j-\omega_at)]. \tag{18}$$

In Eq. (18), we assumed that no streaming is present in the fluid, so the spectral component associated with $n=0$ (dc component) is excluded from the spectrum. Since the dc component is not playing any role in mechanism 2, it is also excluded from the solution for the phase term $\Delta\varphi_{s,n}$.

By combining Eqs. (13)–(15) and (18), we obtain expressions for the values of the phase terms $\Delta\varphi_{s,n}$ and $\Delta\varphi_{s,d}$ for the train of ultrasound pulses

$$\Delta\varphi_{s,n}=i\frac{\Lambda}{4\pi}\sum_{\substack{n=-\infty\\ n\neq0}}^{+\infty}\frac{\eta}{n}\tilde{f}_0\left(\frac{n}{v_aT}\right)\exp(in\omega_at)[\exp(in\omega_a\tau)-1]\times\sum_{j=0}^{N}\frac{1}{\chi_{j+1}}[\exp(-ink_ax_{j+1})-\exp(-ink_ax_j)], \tag{19a}$$

$$\Delta\varphi_{s,d}=-i\frac{\Lambda}{4\pi}\sum_{\substack{n=-\infty\\ n\neq0}}^{+\infty}\frac{S_n\exp(-i\phi_n)}{n}\tilde{f}_0\left(\frac{n}{v_aT}\right)\exp(in\omega_at)\times[\exp(in\omega_a\tau)-1]\sum_{j=1}^{N}(\chi_j-\chi_{j+1})\exp(-ink_ax_j), \tag{19b}$$

where $\Lambda=2n_0k_0P_0/(\rho v_a^2)$.

Since the phase increments associated with the different components of the optical path are correlated in general, it is not appropriate to use the approach of a Gaussian random variable for calculation of $\langle\exp(i\Delta\varphi_s)\rangle_{t,H}$. To simplify the task of averaging the autocorrelation function, we assume, like in the previous work [16], that the total phase perturbation $\Delta\varphi_s$ due to the ultrasound is much less than one radian. In that case, it is sufficient to consider only the first two terms in the development of the exponential function from Eq. (11). The linear term $\langle\Delta\varphi_s\rangle_{t,H}$ in the development is zero for any pulse shape function $f_0(u)$, so, finally, we have

$$\langle\exp(i\Delta\varphi_s)\rangle_{t,H}\approx1-\tfrac{1}{2}\langle\Delta\varphi_s^2\rangle_{t,H}. \tag{20}$$

Note that in the approximation of the small values of $\Delta\varphi_s$, expression $\exp(-\langle\Delta\varphi_s^2\rangle_{t,H}/2)$ is also a good approximation for $\langle\exp(i\Delta\varphi_s)\rangle_{t,H}$, but it cannot be used for estimation of the

higher harmonics unless the phase increments are uncorrelated. This task could be accomplished, for example, by taking into account more terms in Eq. (20).

To obtain the expression for $\langle \Delta\varphi_s^2 \rangle_{t,H}$, we first split the whole term into three parts associated with the ultrasound induced optical index of refraction changes, with the displacements of the scatterers, and with the correlations between these two mechanisms,

$$\langle \Delta\varphi_s^2 \rangle_{t,H} = \langle \Delta\varphi_{s,n}^2 \rangle_{t,H} + \langle \Delta\varphi_{s,d}^2 \rangle_{t,H} + \langle 2\Delta\varphi_{s,n}\Delta\varphi_{s,d} \rangle_{t,H}. \tag{21}$$

Among the terms $\Delta\varphi_{s,d}^2$, $\Delta\varphi_{s,n}^2$, and $2\Delta\varphi_{s,d}\Delta\varphi_{s,n}$, after averaging over time, only those which contain products $\tilde{f}_0[n/(v_aT)]\tilde{f}_0[m/(v_aT)]$ where $n+m=0$ survive. As a result, we have

$$\langle \Delta\varphi_{s,n}^2 \rangle_t = \left(\frac{\Lambda}{2\pi}\right)^2 \sum_{\substack{n=-\infty \\ n\neq 0}}^{+\infty} \sin^2\left(\frac{1}{2}n\omega_a\tau\right)\frac{\eta^2}{n^2}\left|\tilde{f}_0\left(\frac{n}{v_aT}\right)\right|^2 \times \sum_{j=0}^{N}\sum_{k=0}^{N} \frac{\exp(ink_ax_{k+1}) - \exp(ink_ax_k)}{\chi_{j+1}\chi_{k+1}} \times [\exp(-ink_ax_{j+1}) - \exp(-ink_ax_j)], \tag{22a}$$

$$\langle \Delta\varphi_{s,d}^2 \rangle_t = \left(\frac{\Lambda}{2\pi}\right)^2 \sum_{\substack{n=-\infty \\ n\neq 0}}^{+\infty} \sin^2\left(\frac{1}{2}n\omega_a\tau\right)\frac{S_n^2}{n^2}\left|\tilde{f}_0\left(\frac{n}{v_aT}\right)\right|^2 \times \sum_{j=1}^{N}\sum_{k=1}^{N} (\chi_j - \chi_{j+1})(\chi_k - \chi_{k+1}) \times \exp(-ink_ax_j)\exp(ink_ax_k), \tag{22b}$$

$$\langle 2\Delta\varphi_{s,d}\Delta\varphi_{N,n} \rangle_t = -\left(\frac{\Lambda}{2\pi}\right)^2 \sum_{\substack{n=-\infty \\ n\neq 0}}^{+\infty} \sin^2\left(\frac{1}{2}n\omega_a\tau\right)\frac{\eta S_n \exp(i\phi_n)}{n^2} \times \left|\tilde{f}_0\left(\frac{n}{v_aT}\right)\right|^2 \sum_{j=0}^{N}\sum_{k=1}^{N} \frac{\chi_k - \chi_{k+1}}{\chi_{j+1}} \exp(ink_ax_k) \times [\exp(-ink_ax_{j+1}) - \exp(-ink_ax_j)]. \tag{22c}$$

For each frequency n/T, averaging over all free path lengths l_j between consecutive scatterers and averaging over all scattering angles χ_j can be done in the same way as in Ref. [18], to obtain

$$\langle \Delta\varphi_{s,n}^2 \rangle_{t,H} = \frac{\Lambda^2}{\pi^2}\sum_{n=1}^{+\infty} \sin^2\left(\frac{1}{2}n\omega_a\tau\right)\frac{\eta^2}{n^2}\left|\tilde{f}_0\left(\frac{n}{v_aT}\right)\right|^2 \times (k_anl)^2\,\mathrm{Re}[(N+1)\hat{J}_n(\hat{I}-\hat{J}_n)^{-1} - (\hat{J}_n^2 - \hat{J}_n^{N+3})(\hat{I}-\hat{J}_n)^{-2}]_{0,0}, \tag{23a}$$

$$\langle \Delta\varphi_{s,d}^2 \rangle_{t,H} = \frac{\Lambda^2}{\pi^2}\sum_{n=1}^{+\infty} \sin^2\left(\frac{1}{2}n\omega_a\tau\right)\frac{S_n^2}{n^2}\left|\tilde{f}_0\left(\frac{n}{v_aT}\right)\right|^2 \times \left[N\frac{1-g_1}{3} - \frac{(1-g_1)^2}{(k_anl)^2}[1 - \mathrm{Re}\,(\hat{J}_n^{N-1})_{0,0}]\right], \tag{23b}$$

$$\langle 2\Delta\varphi_{s,d}\Delta\varphi_{N,n} \rangle_{t,H} = \frac{\Lambda^2}{\pi^2}\sum_{n=1}^{+\infty} \sin^2\left(\frac{1}{2}n\omega_a\tau\right)\frac{2\eta S_n\cos(\phi_n)}{n^2} \times \left|\tilde{f}_0\left(\frac{n}{v_aT}\right)\right|^2 (1-g_1) \times \{-N + \mathrm{Re}\,[\hat{J}_n(\hat{I}-\hat{J}_n^N)(\hat{I}-\hat{J}_n)^{-1}]_{0,0}\}. \tag{23c}$$

In Eq. (23), $\hat{I}$ is the identity matrix; the (i,j) element of the matrix $\hat{J}_n$ is defined as

$$[\hat{J}_n]_{(i,j)} = g_i^{1/2}g_j^{1/2}\sqrt{\frac{2i+1}{2}}\sqrt{\frac{2j+1}{2}}\int_{-1}^{1} T_n(x)P_i(x)P_j(x)dx, \tag{24}$$

where $T_n(x)=(1-ik_anlx)^{-1}$; $P_j(x)$ is the jth Legendre polynomial; $\mathrm{Re}(\,)_{0,0}$ represents the real part of the (0,0) element of the matrix; and the g_m's are the coefficients in the phase function development from Eq. (10).

For a large number of scattering events N along the path of length s in diffusion regime, we can approximate Eq. (23) by replacing the N with its average value s/l. We finally have

$$\langle \Delta\varphi_{s,n}^2 \rangle_{t,H} = \sum_{n=1}^{+\infty} \sin^2\left(\frac{n\pi\tau}{T}\right)C_n(n), \tag{25a}$$

$$\langle \Delta\varphi_{s,d}^2 \rangle_{t,H} = \sum_{n=1}^{+\infty} \sin^2\left(\frac{n\pi\tau}{T}\right)C_d(n), \tag{25b}$$

$$\langle 2\Delta\varphi_{s,n}\Delta\varphi_{s,d} \rangle_{t,H} = \sum_{n=1}^{+\infty} \sin^2\left(\frac{n\pi\tau}{T}\right)C_{n,d}(n), \tag{25c}$$

where the C terms $[C_n(n)$, $C_d(n)$, and $C_{n,d}(n)]$, represent the amplitudes of the average of the squares of the phase terms at each ultrasound frequency,

$$C_n(n) = \frac{\Lambda^2}{\pi^2}\left|\tilde{f}_0\left(\frac{n}{v_aT}\right)\right|^2\frac{\eta^2}{n^2}(k_anl)^2\mathrm{Re}\left[\left(\frac{s}{l}+1\right)\hat{J}_n(\hat{I}-\hat{J}_n)^{-1} - \hat{J}_n{}^2(\hat{I}-\hat{J}_n{}^{s/l+1})(\hat{I}-\hat{J}_n)^{-2}\right]_{0,0}, \tag{26a}$$

$$C_d(n) = \frac{\Lambda^2}{\pi^2}\left|\tilde{f}_0\left(\frac{n}{v_aT}\right)\right|^2\frac{S_n^2}{n^2}\left(\frac{s}{l}\frac{1-g_1}{3} - \frac{(1-g_1)^2}{(k_anl)^2} \times \mathrm{Re}(\hat{I}-\hat{J}_n{}^{s/l-1})_{0,0}\right), \tag{26b}$$

$$C_{n,d}(n) = \frac{\Lambda^2}{\pi^2}\left|\tilde{f}_0\left(\frac{n}{v_a T}\right)\right|^2 \frac{2\eta S_n \cos(\phi_n)}{n^2}(1-g_1) \times\left(-\frac{s}{l} + \mathrm{Re}[\hat{J}_n(\hat{I}-\hat{J}_n^{s/l})(\hat{I}-\hat{J}_n)^{-1}]_{0,0}\right). \tag{26c}$$

It can be shown by numerical calculation that for a given path length s, the value of each C term in Eq. (26) is approximately independent from particular values of the optical mean free path l and anisotropy factor g_1, as long as the transport mean free path $l/(1-g_1)$ remains constant. This extends the conclusion about the similarity relation made in the case of large $k_a l$ values [18] to the case of small $k_a l$ values, too. For simplicity, in future analysis we will consider only isotropic scattering, noting that the anisotropic case can be approximately reduced to isotropic by replacing the l in the isotropic equations with the value of $l_{tr}=l/(1-g_1)$. Also, we will frequently refer to the transport mean free path when making observations about the $k_a l$ dependence of the C terms, although the mean free path will be used in isotropic equations for simplicity. In the isotropic case, matrix $\hat{J}_n$ reduces to its (0,0) element, $G_n=(nk_a l)^{-1}\arctan(nk_a l)$, and the values of the C terms become

$$C_n(n) = \frac{\Lambda^2}{\pi^2}\left|\tilde{f}_0\left(\frac{n}{v_a T}\right)\right|^2 \frac{\eta^2}{n^2}(k_a n l)^2\left[\left(\frac{s}{l}+1\right)\frac{G_n}{1-G_n} - \frac{G_n^2(1-G_n^{s/l+1})}{(1-G_n)^2}\right], \tag{27a}$$

$$C_d(n) = \frac{\Lambda^2}{\pi^2}\left|\tilde{f}_0\left(\frac{n}{v_a T}\right)\right|^2 \frac{S_n^2}{n^2}\left(\frac{s}{3l} - \frac{1-G_n^{s/l-1}}{(k_a n l)^2}\right), \tag{27b}$$

$$C_{n,d}(n) = \frac{\Lambda^2}{\pi^2}\left|\tilde{f}_0\left(\frac{n}{v_a T}\right)\right|^2 \frac{2\eta S_n \cos(\phi_n)}{n^2}\left(-\frac{s}{l} + \frac{G_n(1-G_n^{s/l})}{(1-G_n)}\right). \tag{27c}$$

III. AUTOCORRELATION FUNCTION DEPENDENCE ON ULTRASOUND FREQUENCY

A broadband ultrasound pulse has energy spread over a wide range of ultrasonic frequencies. In this section, we present a more detailed analysis of the ultrasound frequency dependence of the acousto-optical signal in optically diffusive media.

We focus here on the single frequency component in a general solution obtained in Sec. II B. For conciseness, we look at the special case of the train of ultrasonic pulses when it represents an actual monochromatic plane ultrasound wave (CW). The CW case solution can be obtained from Eq. (27) if we first select the pulse shape function $f_0(u)$ to be equal to zero everywhere except in the interval $(-\pi/\hat{k}_a, \pi/\hat{k}_a)$, where it is equal to one sinusoidal cycle

$$f_0(u) = \begin{cases} \sin(\hat{k}_a u), & u \in (-\pi/\hat{k}_a, \pi/\hat{k}_a), \\ 0, & \text{elsewhere}. \end{cases} \tag{28}$$

Then, we take the limit $\hat{k}_a \to k_a$, where k_a is the magnitude of the ultrasonic wave vector associated with the period between ultrasonic pulses. In the limiting case, the pressure propagation function, $f(x,t)$ defined in Eq. (4), is reduced to a pure sinusoidal function. The Fourier transform of $f_0(u)$ for discreet frequencies $\nu=n/(v_a T)$ and in a limiting case $\hat{k}_a \to k_a$, is zero for all n except when $n=1$. For $n=1$, we have $\tilde{f}_0[1/(v_a T)]=iv_a T/2$, and the set of Eqs. (27) simplifies to the solution for the CW case

$$\langle \Delta\varphi_{s,n}^2\rangle_{t,H} = \sin^2\left(\tfrac{1}{2}\omega_a\tau\right)C_n, \tag{29a}$$

$$\langle \Delta\varphi_{s,d}^2\rangle_{t,H} = \sin^2\left(\tfrac{1}{2}\omega_a\tau\right)C_d, \tag{29b}$$

$$\langle 2\Delta\varphi_{s,n}\Delta\varphi_{s,d}\rangle_{t,H} = \sin^2\left(\tfrac{1}{2}\omega_a\tau\right)C_{n,d}, \tag{29c}$$

where

$$C_n = \Lambda^2\frac{\eta^2}{k_a^2}(k_a l)^2\left[\left(\frac{s}{l}+1\right)\frac{G}{1-G} - \frac{G^2(1-G^{s/l+1})}{(1-G)^2}\right], \tag{30a}$$

$$C_d = \Lambda^2\frac{S^2}{k_a^2}\left(\frac{s}{3l} - \frac{1-G^{s/l-1}}{(k_a l)^2}\right). \tag{30b}$$

$$C_{n,d} = \Lambda^2\frac{2\eta S\cos(\phi)}{k_a^2}\left(-\frac{s}{l} + \frac{G(1-G^{s/l})}{1-G}\right). \tag{30c}$$

In Eq. (30), the subscript n is removed from G_n, S_n, and ϕ_n, since all of them are calculated at the same ultrasound frequency, i.e., when $n=1$. These expressions are generalizations of the previously derived theory [16,18] to cases where the optical transport mean free path is smaller than the ultrasonic wavelength. Therefore, in Eq. (30), not only the parts that are linear with s/l are presented, but, also, the terms that are a result of strong correlation among the optical phase increments due to the different scattering events and among the optical phase increments due to the different optical free paths between consecutive scatterers. Another important difference is that we have significant correlation between the phase increments due to mechanism 1 and mechanism 2, unless the cosines of the phase lag between the ultrasound induced movement of the scatterers and the fluid is exactly zero. This correlation is represented in the mixed term given by Eq. (29c), and it is not zero even for large values of the $k_a l$ product when the correlations vanish between phase increments due to only mechanism 1 or only mechanism 2. This result can be explained in the following way: at each scatterer position, the phase increment that is due to displacement can be approximated as a sum of the two terms associated with the incoming and outgoing scattering directions. Each free path between two consecutive scatterers is associated with two such displacement terms. The phase of the sum of these two displacement terms differs from the phase of the index of refraction term associated with the

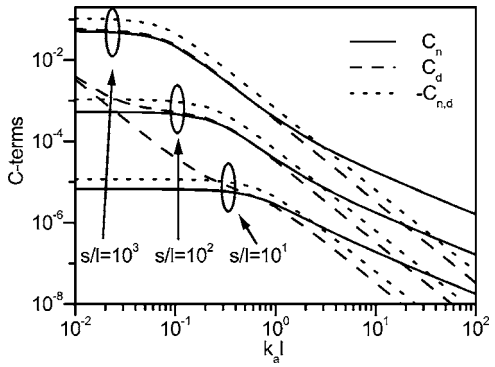

FIG. 1. Dependence of the C terms on the ultrasound frequency. Index of refraction term C_n, displacement of the scatterers term C_d, and mixed term $C_{n,d}$ multiplied by -1, are presented for three different s/l values. The values of the parameters used are $l=1$ mm, $\Lambda=1$ m^{-1}, $\eta=0.32$, $S=1$, and $\phi=0$.

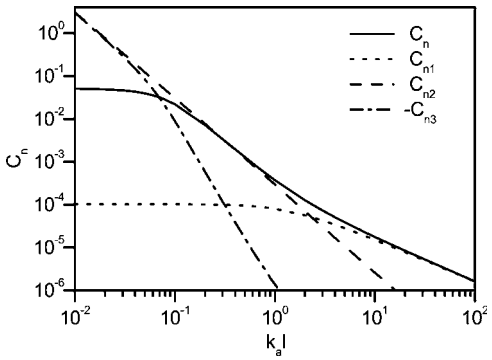

FIG. 2. Dependence of the components of the C_n term on the ultrasound frequency, for $s/l=10^3$. The values of the parameters used are $l=1$ mm, $\Lambda=1$ m^{-1}, $\eta=0.32$, $S=1$, and $\phi=0$.

corresponding free path by exactly $\pi+\phi$, where ϕ is the phase lag between the fluid and the scatterer movement. Therefore, the product of these terms is negative, and its average is not zero unless $\cos(\phi)=0$. The strength of the correlation is proportional to the $\cos(\phi)$, as can be seen from Eq. (30c). For smaller $k_a l$ values, when the length of the ultrasound wave increases in respect to the optical transport mean free path, correlations also appear between the optical phase increments associated with several consecutive displacement and index of refraction terms.

Figure 1 presents the ultrasound frequency dependence of C terms in Eq. (30) for several values of the average number of scattering events s/l along the optical path. The values of the C terms at $s/l=10$ are presented for completeness, although the applied approximations may not be valid for such a small average number of scattering events along the optical path. The parameters used in the calculation are optical mean free path $l=1$ mm; elasto-optic coefficient of water at room temperature $\eta=0.32$; $\Lambda=1$ m^{-1}; and it is assumed that the scatterers are exactly following the fluid displacement ($S=1, \phi=0$). The term $C_{n,d}$ is multiplied by -1 to be presented on the same graph with the other two terms, although its value is negative and it actually cancels out, to some extent, the phase accumulations due to the individual contributions of the two mechanisms of modulation. It is important to notice that each C term in Eq. (30) is not an explicit function of only the $k_a l$ product, regardless of the specific values of k_a and l. However, the ratio between each two C terms in Eq. (30) for a given s/l ratio depends only on the $k_a l$ product, up to a multiplication constant which depends on η, S, and $\cos(\phi)$.

The index of refraction term C_n, and the displacement term C_d have quite different behaviors at the opposite ends of the $k_a l$ range, as can be seen from Fig. 1. When the ultrasound pressure amplitude is constant, except for some intermediate interval of the $k_a l$ values, C_d is proportional to the square of the scatterer displacement amplitude (i.e., inversely proportional to the square of the ultrasound frequency). When the $k_a l$ product is small, scatterers along the optical path occupy a space volume where the ultrasound phase is nearly the same, unless the value of s/l is very large. The C_d term in that region depends very little on l and s. When the scatterers are within the same ultrasound phase, we have a cancellation of the optical phase increments due to mechanism 1 which share the same free path between consecutive scatterers. Then, only increments from the first incoming direction χ_1, and the last outgoing direction χ_{N+1} contribute to C_d, and it behaves as if it was caused by only one scatterer. In contrary, if we choose the source and detector positions to move with the ultrasound, then, we essentially have cancellation between all of the displacement contributions in the limit of low $k_a l$ values. On the other side of the $k_a l$ range, when the optical transport mean free path is greater than the ultrasound wavelength, the phase increments between different scattering events are uncorrelated. In that region, the C_d term is equal to the sum of the individual scattering contributions, which are all proportional to k_a^{-2}.

The behavior of the C_n term is particularly interesting since the correlations between the phase increments from different free paths are present for much higher ultrasound frequencies than in the case of the C_d term. Figure 2 presents the C_n dependence on the ultrasound frequency for $(s/l)=10^3$. We present the C_n as a sum of three terms, $C_{n1}+C_{n2}+C_{n3}$, which are given by

$$C_{n1}=\Lambda^2\frac{\eta^2}{k_a^2}(k_a l)^2\left[\left(\frac{s}{l}+1\right)G\right], \tag{31a}$$

$$C_{n2}=\Lambda^2\frac{\eta^2}{k_a^2}(k_a l)^2\left[\left(\frac{s}{l}+1\right)\frac{G^2}{1-G}\right], \tag{31b}$$

$$C_{n3}=\Lambda^2\frac{\eta^2}{k_a^2}(k_a l)^2\left[-\frac{G^2(1-G^{s/l+1})}{(1-G)^2}\right]. \tag{31c}$$

The first two terms C_{n1} and C_{n2} were derived previously [16,18] for the case where the $k_a l$ values were large enough that we could neglect the terms which were not linearly proportional to s/l. The term C_{n1} (dotted line in Fig. 2) is the result of averaging the individual squares of the phase accumulations along the free paths. It is proportional to the average number of free paths $s/l+1$, and it has a transition from a weak dependence on $k_a l$ (in a low $k_a l$ region) to $(k_a l)^{-1}$ dependence for large $k_a l$. The term C_{n2} (dashed line on Fig.

2) is proportional to $s/l+1$, and it is a part of the result of averaging the products between the phase accumulations along the different free paths. This term has approximately $(k_a l)^{-2}$ dependence. Finally, term C_{n3} is nonlinear with the s/l part of the result of averaging the products between the phase accumulations along the different free paths. It is a result of strong correlation between the phase accumulations along the different free paths for low $k_a l$ values. It has a negative value, so the dashed-doted line in Fig. 2 presents the $k_a l$ dependence of $-C_{n3}$. The term C_{n1} eventually dominates all of the other contributions to C_n when $k_a l$ is sufficiently large, suggesting that the optical phase increments from the different free paths that are due to mechanism 2 are completely uncorrelated. For the lower $k_a l$ values, the correlations between the phase accumulations along the different free paths begin to dominate in the C_n term—first through term C_{n2} which is proportional to s/l, and then combined with the C_{n3}. When $k_a l$ is low enough that all of the scatterers occupy space with the similar ultrasound phase, then the increments from the different free paths add constructively. The C_n term in that limit becomes less dependent on k_a and l and more dependent on the square of the total path length s^2.

Finally, in a case of $C_{n,d}$, when $k_a l$ is sufficiently large, we also have an absence of correlation between the phase increments due to mechanisms 1 and 2 for the components of the optical path that do not share the same free path. However, as described earlier, the correlation between the phase increments due to mechanisms 1 and 2 for the same free path between two consecutive scatterers is always present, unless the cosines of the phase lag between the ultrasound induced movement of the scatterers and the fluid is exactly zero.

It is interesting to compare the intensities of the first sidebands of the acousto-optically modulated light when it propagates the same length L in optically clear and optically turbid media. In particular, with the optically clear media, we assume that the light and the ultrasound are traveling along the x and z directions, respectively, and that conditions for the Raman-Nath diffraction are satisfied. In a formal Raman-Nath approach [32], the phase of the electrical field accumulated along the interaction length L is equal to

$$\varphi(t) = k_0 n_0 L\left[1 + \tfrac{1}{2} M \cos(\omega_a t - k_a z)\right]. \tag{32}$$

In Eq. (32), $\omega_a = 2\pi f_a$, where f_a is the ultrasound frequency, and $M = 2\eta P_0/(\rho v_a^2)$ is, like in Eq. (7), related to the optical index of refraction change that is due to the ultrasound. We proceed with developing the electrical field in analytic signal representation, using Bessel functions and calculating the autocorrelation function $<E(t+\tau)E^*(t)>_t$. It is assumed that the amplitude of the electrical field is unity and that the phase disturbance is small enough that the Bessel functions can be approximated with the linear and quadratic terms. If we limit the solution to only the first harmonics, the expression for the power spectral density $\mathcal{P}(\nu)$ is

$$\mathcal{P}(f) = \left(1 - \tfrac{1}{4} C_{\mathrm{RN}}\right)\delta(f - f_0) + \tfrac{1}{8} C_{\mathrm{RN}}\delta(f - f_0 + f_a) + \tfrac{1}{8} C_{\mathrm{RN}}\delta(f - f_0 - f_a). \tag{33}$$

In Eq. (33), f_0 is the frequency of unmodulated light; $\delta(\,)$ is the Dirac delta function; and the parameter C_{RN} is equal to $\Lambda^2 L^2 \eta^2/2$.

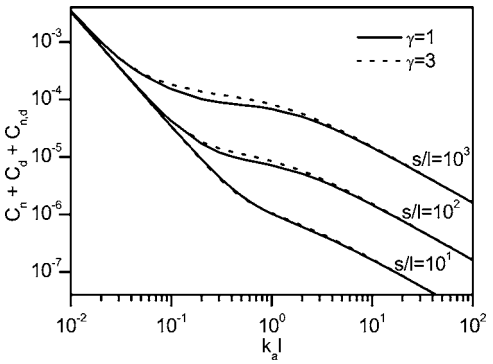

FIG. 3. Ultrasound frequency dependence of the sum of the C terms, for two different values of the mass density ratio γ. Values of the parameters are scatterer radius $a_0 = 1$ μm, optical mean free path $l = 1$ mm, kinematic viscosity of water $\eta_k = 10^{-6}$ m^2 s^{-1}, elasto-optic coefficient of water $\eta = 0.32$, and $\Lambda = 1$ m^{-1}.

In the optically multiple scattering regime described in Eq. (29), based on Eqs. (11) and (20), the power spectral density for the path of length L is given by the same type of equation as Eq. (33), where parameter C_{RN} is replaced with the sum $C = C_n + C_d + C_{n,d}$ and pathlength L is substituted for s. For low $k_a l$ values, C_d is the dominant term in the sum. In that range of $k_a l$ values, $G \approx 1 - (k_a l)^2/3$, and, consequently, $C_d \approx \Lambda^2 S^2/(3k_a^2)$. This result implies that the C_d term behaves like a displacement contribution from a single scatterer. It is, therefore, dependent on k_a^{-2}, and only slightly dependent on pathlength L. In the same regime of low $k_a l$ values, $C_n \approx C_{\mathrm{RN}}$. This is in agreement with the fact that in the limit of low $k_a l$ values, all of the scatterers are within a space with almost the same phase of the ultrasound field, and the contributions from mechanism 2 add constructively, regardless of different scattering directions. On the contrary, when $k_a l$ is large, the values of the C terms are significantly lower than C_{RN} due to the increased cancellation of the phase increments. In that regime, $G \approx \pi/(2k_a l)$ and all of the C terms are well described with their parts linearly proportional to s/l. The C_n term is then proportional to k_a^{-1}, and it is lower than C_{RN} by a ratio of s/λ_a, where λ_a is the ultrasound wavelength. Compared to the C_n term, the C_d and $C_{n,d}$ terms are lower by another l/λ_a ratio, discarding the parameters η, S, and $\cos(\phi)$ involved in their expressions. Both parameters depend on k_a^{-2}, and their contribution to the sum C is not important compared to C_n.

Finally, we plot in Fig. 3 the ultrasonic frequency dependence of the sum C of the optical phase accumulation terms, C_n, C_d, and $C_{n,d}$, for two different relative mass densities of the optical scatterers ($\gamma = 1$ and $\gamma = 3$) and three different values of s/l. We choose the mean optical scattering free path to be $l = 1$ mm and the radius of the optical scatterers as $a_0 = 1$ μm. For this set of chosen parameters, in the range of the small $k_a l$ values, the particles are following the fluid displacement in amplitude and phase ($S \approx 1$ and $\phi \approx 0$), and there is no noticeable difference between the values of the C term for the different γ values. With a large $k_a l$, the C term follows the behavior of the index of refraction term C_n, and

the influence of the C_d term is small. Therefore, only in the range of intermediate $k_a l$ values, where both a phase and an amplitude difference between the scatterers and fluid motion exist (for $\gamma=3$), and where the C_d term contributes significantly to the value of C, does a discrepancy appear between the values of the C term for different γ values. We expect that γ is just slightly different from unity in most situations in real biological soft tissues, in which case the observed discrepancy is not significant.

We mentioned earlier that when $k_a l$ is large, the C term is dominated by the value of the index of refraction term C_n, and it is dependent on the k_a^{-1}. Interestingly, when $k_a l$ is small, the value of the elasto-optic coefficient η in water is such that a large cancellation occurs when summing the C terms, due to the negative value of $C_{n,d}$. As a result, in a low $k_a l$ limit, the C term behaves like the C_d term at low values of s/l, i.e., as if it is caused by the displacement contribution of only one scatterer.

Note that the value of the Λ parameter is proportional to the acoustic pressure amplitude P_0, and, consequently, the modulated intensity has a P_0^2 dependence. From Fig. 3, in the CW regime, when $k_a l$ is small, pressure amplitude values as low as $P_0=1$ kPa are sufficient to produce values of the C term that are close to unity, which is at the edge of acceptance for our theory based on the small phase approximation. When propagating ultrasound pulses, we can apply significantly higher peak ultrasound pressures without violating the assumption of small phase increments.

IV. TRANSMISSION AND REFLECTION OF THE ACOUSTO-OPTICALLY MODULATED LIGHT INTENSITY IN A SLAB GEOMETRY

A. Slab equations

In this section, we present the analytical expression for an acousto-optical signal produced by a train of ultrasound pulses in the case of an infinitely wide optically scattering slab. Since it is possible to find a reasonably good analytical expression for the pathlength probability density function for both transmission and reflection slab geometry, a slab has been considered previously for various problems [3,16,17,28,33–35]. We choose the Z axis of the coordinate system to be perpendicular to the infinitely wide slab of thickness d. The indices of refraction of both the surrounding and scattering media are n_0. A plane ultrasonic wave propagates within the slab (in the X-Y plane) and is assumed to fill the whole slab. We consider two cases. In the first case, which we will refer to as the transmission case, one side of the slab is irradiated by a plane electromagnetic wave, and a point detector measures the optical intensity on the side of the slab opposite to the light source. By solving the diffusion equation for this geometry, it is possible to find an expression [16,33,35] for the photon pathlength probability density function $p(s)$. For the transmission case, we follow the derivation of $p(s)$ from [16,33] by applying an infinite number of image sources and introducing extrapolated-boundary conditions [33,35]. We assume isotropic scattering, in which case, $\mu_s'=\mu_s$. By virtue of the similarity relation described in Sec. II B, we can extend the conclusions obtained from the isotropic case to anisotropic scattering also. The final expression for the probability density function $p_T(s)$ for the path of length s in the transmission geometry is

$$p_T(s) = K_T(s)\sum_{n=1}^{+\infty}\left[[(2n-1)d_0 - z_0]\exp\left(-\frac{[(2n-1)d_0 - z_0]^2}{4Ds}\right) - [(2n-1)d_0 + z_0]\exp\left(-\frac{[(2n-1)d_0 + z_0]^2}{4Ds}\right)\right], \quad (34)$$

where

$$K_T(s) = \frac{\sinh(d_0\sqrt{\mu_a/D})}{\sinh(z_0\sqrt{\mu_a/D})} s^{-3/2}\exp(-\mu_a s)(4\pi D)^{-1/2}. \quad (35)$$

In Eq. (34), the diffusion constant is given by $D=[3(\mu_a+\mu_s)]^{-1}$; d_0 is the distance between the two extrapolated boundaries of the slab; and z_0 is the location of the converted isotropic source from the extrapolated incident boundary of the slab. The distance between the extrapolated boundary and the corresponding real boundary of the slab is $l\gamma^*$, where $\gamma^*=0.7104$ and l is the scattering mean free path ($l=1/\mu_s$). The converted isotropic source is one isotropic scattering mean free path into the slab. Therefore, $d_0=d+2l\gamma^*$, and $z_0=l(1+\gamma^*)$.

In the second (reflection) case, the point detector and the point source of light are positioned on the same side of the slab, and separated from each other by a distance ρ in the X-Y plane. We also assume in this case that the slab is infinitely thick. Similarly to the transmission case, we obtain the solution for the pathlength probability density function $p_R(s)$ in the reflection geometry,

$$p_R(s) = \frac{2\pi^{-1/2}[(z_0^2+\rho^2)/(4D)]^{3/2}}{[1+2\sqrt{\mu_a(z_0^2+\rho^2)/(4D)}]}\exp\left(2\sqrt{\frac{\mu_a(z_0^2+\rho^2)}{4D}}\right) \times s^{-5/2}\exp(-\mu_a s)\exp\left(-\frac{\rho^2+z_0^2}{4Ds}\right). \quad (36)$$

The following expressions are needed in order to perform averaging of the terms in Eq. (26) over the pathlength probabilities:

$$\begin{aligned} T_s &= \int_0^{+\infty} p_T(s)s\,ds, \\ R_s &= \int_0^{+\infty} p_R(s)s\,ds, \\ T_{\exp,n} &= \int_0^{+\infty} p_T(s)\exp(-Q_n s)\,ds, \\ R_{\exp,n} &= \int_0^{+\infty} p_R(s)\exp(-Q_n s)\,ds, \end{aligned} \quad (37)$$

where $Q_n=-\ln(G_n)/l$. After calculating the integrals in Eq. (37), we have

$$T_s = \frac{d_0 \coth(d_0\sqrt{\mu_a/D}) - z_0 \coth(z_0\sqrt{\mu_a/D})}{2\sqrt{\mu_a D}},$$

$$R_s = \frac{\rho^2 + z_0^2}{2D[1 + \sqrt{\mu_a(\rho^2 + z_0^2)/D}]},$$

$$T_{\exp,n} = \frac{\sinh(d_0\sqrt{\mu_a/D})}{\sinh(z_0\sqrt{\mu_a/D})} \frac{\sinh[z_0\sqrt{(\mu_a + Q_n)/D}]}{\sinh[d_0\sqrt{(\mu_a + Q_n)/D}]}, \quad (38)$$

$$R_{\exp,n} = \frac{1 + \sqrt{(\mu_a + Q_n)(\rho^2 + z_0^2)/D}}{1 + \sqrt{\mu_a(\rho^2 + z_0^2)/D}} \times \frac{\exp[-\sqrt{(\mu_a + Q_n)(\rho^2 + z_0^2)/D}]}{\exp[-\sqrt{\mu_a(\rho^2 + z_0^2)/D}]}.$$

If we denote with $\langle C_n(n)\rangle_{s,T}$, $\langle C_d(n)\rangle_{s,T}$, and $\langle C_{n,d}(n)\rangle_{s,T}$ the averages of the appropriate C terms in Eq. (26) over all of the pathslengths in the transmission geometry, we have, with the help of Eq. (38),

$$\langle C_n(n)\rangle_{s,T} = \frac{\Lambda^2}{\pi^2}\left|\tilde{f}_0\left(\frac{n}{v_a T}\right)\right|^2 \frac{\eta^2}{n^2}(k_a n l)^2 \left[\frac{G_n}{1 - G_n}\left(\frac{T_s}{l} + 1\right) - \frac{G_n^2(1 - G_n T_{\exp,n})}{(1 - G_n)^2}\right], \quad (39a)$$

$$\langle C_d(n)\rangle_{s,T} = \frac{\Lambda^2}{\pi^2}\left|\tilde{f}_0\left(\frac{n}{v_a T}\right)\right|^2 \frac{S_n^2}{n^2}\left(\frac{T_s}{3l} - \frac{1 - G_n^{-1} T_{\exp,n}}{(k_a n l)^2}\right), \quad (39b)$$

$$\langle C_{n,d}(n)\rangle_{s,T} = \frac{\Lambda^2}{\pi^2}\left|\tilde{f}_0\left(\frac{n}{v_a T}\right)\right|^2 \frac{2\eta S_n \cos(\phi_n)}{n^2} \times \left(-\frac{T_s}{l} + \frac{G_n(1 - T_{\exp,n})}{1 - G_n}\right). \quad (39c)$$

The expressions for the terms $\langle C_n(n)\rangle_{s,R}$, $\langle C_d(n)\rangle_{s,R}$, and $\langle C_{n,d}(n)\rangle_{s,R}$ averaged in the reflection configuration are identical with the expressions in Eq. (39), with T_s and $T_{\exp,n}$ replaced with R_s and $R_{\exp,n}$, respectively.

B. Various pulse shapes

We present the effects of acousto-optical modulation for two distinct types of the ultrasound pulse shapes. The Gaussian pulse shape (pulse 1) is used as a representative of a pulse with the spectrum centered at the zero frequency. Although just an idealization of the ultrasonic pulse generated in realistic conditions, this is a useful example of acousto-optically modulated light dependence on ultrasound frequency. The second pulse shape function (pulse 2) is produced by modulating the pulse 1 profile with the cosines function, and it is a more realistic example of commonly generated ultrasound pulses. Figure 4(a) presents the time profiles of the pulse shape functions, whose expressions are

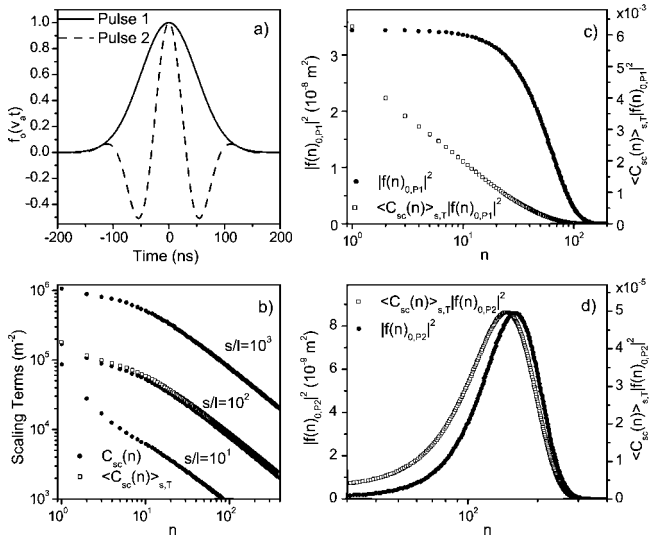

FIG. 4. Frequency spectra of pulses 1 and 2. (a) Pulse time dependence; (b) ultrasound frequency dependence of the scaling terms; (c) power spectrum of the pulse 1 before and after multiplication with the scaling term; (d) power spectrum of the pulse 1 before and after multiplication with the scaling term; parameters used in calculation are index of refraction in water $n_0 = 1.33$; optical wavelength $\lambda_0 = 0.5$ μm; ultrasonic pressure amplitude $P_0 = 10^5$ Pa; speed of sound in water $v_a = 1480$ ms^{-1}; scattering mean free path $l = 1$ mm; elasto-optic coefficient $\eta = 0.32$; relative scatterer density $\gamma = 1$; period between consecutive pulses $T = 20$ μs; pulse 2 central ultrasound frequency $T_u^{-1} = 8$ MHz; $\sigma = 2.5 \times 10^{-3}$.

$$f_{0,P1}(u) = \exp\left(-\frac{u^2}{2(\sigma v_a T)^2}\right), \quad (40a)$$

$$f_{0,P2}(u) = \exp\left(-\frac{u^2}{2(\sigma v_a T)^2}\right)\cos(k_u u). \quad (40b)$$

In Eq. (40), $v_a = 1480$ ms^{-1} is the ultrasound velocity in water; $T = 20$ μs is the time period between pulses; and $\sigma = 2.5 \times 10^{-3}$ is the constant which controls the relative width of each pulse compared to the distance between consecutive pulses, such that both pulses have similar bandwidths ≈ 5.3 MHz. In Pulse 2, k_u is the magnitude of the ultrasound wave vector associated with the 8 MHz central frequency.

Figures 4(c) and 4(d) present the squares of the Fourier transforms of the ultrasound pulse profiles $f_{0,P1}(u)$ and $f_{0,P2}(u)$, for different ultrasound frequencies n/T, respectively,

$$\tilde{f}_{0,P1}\left(\frac{n}{v_a T}\right) = \sigma v_a T\sqrt{2\pi}\exp[-2n^2(\sigma\pi)^2], \quad (41a)$$

$$\tilde{f}_{0,P2}\left(\frac{n}{v_a T}\right) = \sigma v_a T\sqrt{2\pi}\exp[-2n^2(\sigma\pi)^2] \times \exp\left[-2\left(\sigma\pi\frac{T}{T_u}\right)^2\right]\cosh\left(4n(\sigma\pi)^2\frac{T}{T_u}\right), \quad (41b)$$

In calculating the acousto-optical effect, we use the optical wavelength $\lambda_0=0.5$ μm, the optical index of refraction $n_0=1.33$, and the elasto-optic coefficient in water $\eta=0.32$. We also use the scattering mean free path $l=1$ mm, and the optical absorption coefficient $\mu_a=1$ cm^{-1}, which are in agreement with the typical optical transport mean free path and absorption coefficient in soft tissue. Since it is expected that in reality scatterers closely follow the ultrasound induced fluid motion, we use a relative scatterer density γ equal to one. For equal values of the scattering slab thickness in transmission geometry $d=4$ cm, and the distance between the source and the detector in reflection geometry $\rho=4$ cm, and for the particular values of the other parameters used, the probability of the pathlength is almost equal for both the transmission and reflection configurations. Therefore, we present only the transmission case results. We use an ultrasonic pressure amplitude P_0 equal to 10^5 Pa, which is much higher than the allowed CW ultrasound pressure amplitude used in the approximation of small ultrasound modulation. The parameters are also chosen such that the larger ultrasound wavelength in a spectrum is comparable with the slab thickness (or the source-detector distance), and the approximations involved in Eq. (8) are satisfied.

We define the scaling coefficient $C_{sc}(n)$, and the total scaling coefficient $\langle C_{sc}(n)\rangle_{s,T}$ in transmission geometry, at each ultrasound frequency n/T as

$$C_{sc}(n)\left|\tilde{f}\left(\frac{n}{v_aT}\right)\right|^2 = C_n(n) + C_d(n) + C_{n,d}(n), \quad (42a)$$

$$\langle C_{sc}(n)\rangle_{s,T}\left|\tilde{f}\left(\frac{n}{v_aT}\right)\right|^2 = \langle C_n(n)\rangle_{s,T} + \langle C_d(n)\rangle_{s,T} + \langle C_{n,d}(n)\rangle_{s,T}. \quad (42b)$$

Based on Eq. (27), the scaling coefficient $C_{sc}(n)$ scales the power spectral density of the ultrasound pulse train for each particular value of the optical pathlength s. The black squares on Fig. 4(b) present the value of $C_{sc}(n)$ for the different ultrasound frequencies and for three different values of s. The scaling coefficient $C_{sc}(n)$ behaves similarly to the sum of the C terms in the CW case (Sec. III). The open squares in Fig. 4(b) present the frequency dependence of the total scaling coefficient $\langle C_{sc}(n)\rangle_{s,T}$, which is the result of path length averaging of the scaling coefficient $C_{sc}(n)$. At each ultrasound frequency, the power spectrum of the acousto-optically modulated intensity is obtained by scaling the power spectrum of the train of pulses with this coefficient. The $\langle C_{sc}(n)\rangle_{s,T}$ behaves similarly to some $C_{sc}(n)$ term at the average value of the pathlength s. In a high frequency range, it is inversely proportional to the ultrasonic frequency, and in a low frequency range, depending on the average pathlength value, it might become inversely proportional to the ultrasound frequency squared.

The open squares in Figs. 4(c) and 4(d) present the ultrasound frequency dependence of the power spectrum of the modulated light, given by $|\tilde{f}[n/(v_aT)]|^2\langle C_{sc}(n)\rangle_{s,T}$, in transmission geometry for the pulse 1 and pulse 2 cases, respectively. Compared with the power spectra of the pulse shape functions (black circles), both pulses are more attenuated at the higher ultrasound frequencies due to the decay of the total scaling coefficient $\langle C_{sc}(n)\rangle_{s,T}$. Pulse 1 is attenuated strongly at higher frequencies, and it suffers a large reduction in bandwidth. The present theoretical model is not valid for very low values of the k_al product, and the concept of infinite train of pulses allows us to avoid this part of the spectrum even in a case where the single pulse shape function has very low frequency components, as in the pulse 1 case. Consequently, based on this model, it is difficult to predict the spectrum of the optical intensity after interaction with only one pulse with a similar shape. However, based on the presented theoretical derivations, it looks reasonable to us to expect a large bandwidth reduction for a pulse with a spectrum centered at zero frequency. In the case of pulse 2, due to the frequency dependence of the total scaling coefficient, the frequency spectrum of the acousto-optically modulated light is slightly broadened for $\approx$0.3 MHz, and the central frequency is left-shifted by 0.7 MHz. Note, also, that the value of the total scaling coefficient $\langle C_{sc}(n)\rangle_{s,T}$ at the central frequency of pulse 2 is several times smaller than its value at the lowest frequency in the spectrum.

V. CONCLUSION

In conclusion, we have presented an extension of the theory of acousto-optical modulation of multiply scattered diffused light toward the small k_al values, where a strong correlation exists between the ultrasound induced optical phase increments associated with different components of the optical path. It is shown that an approximate similarity relation is valid for this extended range of k_al values. For large k_al values, an inverse linear dependence of the modulated signal on the ultrasound frequency is a consequence of the dominating effect of mechanism 2, while in the low k_al range, depending on the particular values of the average number of scattering events along the pathlength, the signal has a tendency to be even inversely proportional to the square of the ultrasound frequency. The theory is also extended to account for complex scatterer movement in respect to surrounding fluid displacement. It is expected that in cases involving the commonly used ultrasound pressures in medicine, the movement of the optical scatterers in soft biological tissues should not differ significantly from the movement of the surrounding tissue. In this situation, even for large values of the k_al product, a significant correlation between the contributions of mechanism 1 and 2 exists. Finally, we derived an analytical solution for acousto-optical modulation when the train of the ultrasound pulses traverses the scattering media. Examples of two characteristic pulse shapes with zero and nonzero central frequencies are presented in the transmission and reflection geometries. It is shown that the ultrasound frequency dependence of the optical phase variations due to mechanisms 1 and 2 produces a nonuniform deviation of the pulse spectra, as well as decay of the modulated light power in the higher ultrasound frequency ranges.

[1] F. A. Marks, H. W. Tomlinson, and G. W. Brooksby, Proc. SPIE **1888**, 500 (1993).
[2] L.-H. V. Wang, S. L. Jacques, and X. Zhao, Opt. Lett. **20**, 629 (1995).
[3] W. Leutz and G. Maret, Physica B **204**, 14 (1995).
[4] M. Kempe, M. Larionov, D. Zaslavsky, and A. Z. Genack, J. Opt. Soc. Am. A **14**, 1151 (1997).
[5] L.-H. V. Wang and G. Ku, Opt. Lett. **23**, 975 (1998).
[6] S. Leveque, A. C. Boccara, M. Lebec, and H. Saint-Jalmes, Opt. Lett. **24**, 181 (1999).
[7] G. Yao, S.-L. Jiao, and L.-H. V. Wang, Opt. Lett. **25**, 734 (2000).
[8] A. Lev, Z. Kotler, and B. G. Sfez, Opt. Lett. **25**, 378 (2000).
[9] M. Hisaka, T. Sugiura, and S. Kawata, J. Opt. Soc. Am. A Opt. Image Sci. Vis **18**, 1531 (2001).
[10] J. Li, G. Ku, and L.-H. V. Wang, Ophthalmic Physiol. Opt. **41**, 6030 (2002).
[11] A. Lev and B. G. Sfez, Opt. Lett. **28**, 1549 (2003).
[12] M. Gross, P. Goy, and M. Al-Koussa, Opt. Lett. **28**, 2482 (2003).
[13] S. Sakadzic and L.-H. V. Wang, Opt. Lett. **29**, 2770 (2004).
[14] T. W. Murray, L. Sui, G. Maguluri, R. A. Roy, A. Nieva, F. Blonigen, and C. A. DiMarzio, Opt. Lett. **29**, 2509 (2004).
[15] F. Ramaz, B. C. Forget, M. Atlan, A. C. Boccara, M. Gross, P. Delaye, and G. Roosen, Opt. Express **12**, 5469 (2004).
[16] L. V. Wang, Phys. Rev. Lett. **87**, 043903 (2001).
[17] L.-H. V. Wang, Opt. Lett. **26**, 1191 (2001).
[18] S. Sakadzic and L. V. Wang, Phys. Rev. E **66**, 026603 (2002).
[19] A. Lev and B. Sfez, J. Opt. Soc. Am. A **20**, 2347 (2003).
[20] G. Yao and L.-H. V. Wang, Appl. Opt. **43**, 13201326 (2004).
[21] M. R. Maxey and J. J. Riley, Phys. Fluids **26**, 883 (1982).
[22] E. E. Michaelidis, J. Fluids Eng. **119**, 233 (1997).
[23] A. T. Hjelmfelt and L. F. Mockros, Appl. Sci. Res. **16**, 149 (1966).
[24] D. A. Siegel and A. J. Plueddemann, J. Atmos. Ocean. Technol. **8**, 296 (1991).
[25] R. N. Zitter, J. Acoust. Soc. Am. **43**, 864 (1968).
[26] T. H. Neighbors and W. G. Mayer, J. Acoust. Soc. Am. **74**, 146 (1983).
[27] J. W. Goodman, *Statistical Optics* (Wiley, New York, 1985).
[28] G. Maret and P. E. Wolf, Z. Phys. B: Condens. Matter **65**, 409 (1987).
[29] D. J. Pine, D. A. Weitz, G. Maret, P. E. Wolf, E. Herbolzheimer, and P. M. Chakin, *Scattering and Localization of Classical Waves in Random Media* (World Scientific, Singapore, 1990).
[30] M. Rosenbluh, M. Hoshen, I. Freund, and M. Kaveh, Phys. Rev. Lett. **58**, 2754 (1987).
[31] B. J. Ackerson, R. L. Dougherty, and N. M. Reguigui J. Thermophys. Heat Transfer **6**, 577 (1992).
[32] A. Korpel, *Acousto-Optics* (Marcel Dekker, Ney York, 1997).
[33] M. S. Patterson, B. Chance, and B. C. Willson, Appl. Opt. **28**, 2331 (1989).
[34] D. J. Pine, D. A. Weitz, P. M. Chaikin, and E. Herbolzheimer, Phys. Rev. Lett. **60**, 1134 (1988).
[35] A. Ishimaru, *Wave Propagation and Scattering in Random Media* (Academic, New York, 1978).